Dynamic Ensemble Coding of Saccades in the Monkey Superior Colliculus

H.H.L.M. Goossens and A. J. Van Opstal

JN 95:2326-2341, 2006. First published Dec 21, 2005; doi:10.1152/jn.00889.2005

J Neurophysiol 95: 2326–2341, 2006.
First published December 21, 2005; doi:10.1152/jn.00889.2005.

Dynamic Ensemble Coding of Saccades in the Monkey Superior Colliculus

H.H.L.M. Goossens and A. J. Van Opstal

Department of Medical Physics and Biophysics, Institute for Neuroscience, Radboud University Nijmegen Medical Center, Nijmegen, The Netherlands

Submitted 24 August 2005; accepted in final form 10 December 2005

Goossens, H.H.L.M. and A. J. Van Opstal. Dynamic ensemble coding of saccades in the monkey superior colliculus. *J Neurophysiol* 95: 2326–2341, 2006. First published December 21, 2005; doi:10.1152/jn.00889.2005. The deeper layers of the midbrain superior colliculus (SC) contain a topographic motor map in which a localized population of cells is recruited for each saccade, but how the brain stem decodes the dynamic SC output is unclear. Here we analyze saccade-related responses in the monkey SC to test a new dynamic ensemble-coding model, which proposes that each spike from each saccade-related SC neuron adds a fixed, site-specific contribution to the intended eye movement command. As predicted by this simple theory, we found that the cumulative number of spikes in the cell bursts is tightly related to the displacement of the eye along the ideal straight trajectory, both for normal saccades and for strongly curved, blink-perturbed saccades toward a single visual target. This dynamic relation depends systematically on the metrics of the saccade displacement vector, and can be fully predicted from a quantitative description of the cell's classical movement field. Furthermore, we show that a linear feedback model of the brain stem, which is driven by dynamic linear vector summation of measured SC firing patterns, produces realistic two-dimensional (2D) saccade trajectories and kinematics. We conclude that the SC may act as a nonlinear, vectorial saccade generator that programs an optimal straight eye-movement trajectory.

INTRODUCTION

The midbrain superior colliculus (SC) is a sensorimotor interface that is critically involved in the control of rapid gaze shifts. An important problem in understanding its role in gaze control is how the spatial distribution of movement-related activity in its motor map is ultimately transformed into the temporal code carried by motor neurons (Sparks and Hartwich-Young 1989). In this study, we analyzed saccade-related responses in the monkey SC to test a new theoretical framework for the involvement of the SC in the generation of saccades in two dimensions (2D). First, we present a novel analysis of SC spike trains that provides evidence for dynamic vector summation of movement contributions provided by each spike of each cell in the active population. We then analyze the spatial-temporal distribution of SC activity. The results are used to test the predictions and emerging properties of our new ensemble-coding theory, which assumes dynamic, linear decoding of the SC population activity by the brain stem saccade generator. Finally, we propose and test a new quantitative description of dynamic SC movement fields that is implied by our theory. In what follows, we first explain why a new approach is called for by highlighting the main findings that have led to several controversies. These controversies include *1*) static versus dynamic involvement of the SC, *2*) vector summation versus vector averaging of the population activity, and *3*) feedforward versus feedback involvement of the SC.

Earlier theories and controversies

Early saccade models (Fig. 1*A*) assumed that localized activity in the SC motor map determines only the eye-centered coordinates of the saccade goal and that the instantaneous trajectory and velocity of the eye are controlled by a nonlinear local feedback loop in the brain stem (Jürgens et al. 1981; Scudder 1988; Van Gisbergen et al. 1981). The mechanism by which the place-coded movement vector of the SC population is converted into a temporal eye displacement input for the brain stem saccade generator was proposed to rely on vector averaging (Lee et al. 1988) rather than on linear vector summation of the individual cell contributions (Van Gisbergen et al. 1987). In this way, the levels of activity within the active cell population would have no direct relation to the saccade trajectory and kinematics.

Note, however, that vector averaging is a nonlinear operation for which it is not obvious how it could be achieved through fixed connections between the SC and the brain stem (Badler and Keller 2002; Bozis and Moschovakis 1998; Groh 2001; Van Opstal and Van Gisbergen 1989). Moreover, the vector-averaging premise for the spatial-to-temporal transformation does not account for the "stretching" of horizontal and vertical saccade components that is needed to obtain straight oblique saccades. Additional assumptions are necessary to explain this behavior (Grossman and Robinson 1988; Van Gisbergen and Van Opstal 1989; Van Gisbergen et al. 1985).

Furthermore, accumulating evidence has indicated that the levels of movement-related activity in the SC do influence the saccade kinematics. For example, low firing rates in the SC are associated with slow saccades (Berthoz et al. 1986; Van Opstal and Van Gisbergen 1990). Also, the intensity, number, and frequency of electrical microstimulation pulses have a systematic effect on both the amplitude and the velocity of saccades evoked at a particular SC site (Stanford et al. 1996; Van Opstal et al. 1990). In addition, the instantaneous discharge of many SC neurons was reported to encode dynamic motor error (Munoz and Wurtz 1995b; Munoz et al. 1991; Waitzman et al. 1991). The latter findings prompted new theories (Lefévre and Galiana 1992; Grossberg et al. 1997; Guitton et al. 2003; Munoz and Wurtz 1995b; Munoz et al. 1991; Waitzman et al. 1991; Wurtz and Optican 1994), which proposed that the local feedback loop is closed through the SC (Fig. 1*B*).

Address for reprint requests and other correspondence: H.H.L.M. Goossens, Dept. of Medical Physics and Biophysics, Inst. for Neuroscience, Radboud Univ. Nijmegen Medical Ctr., Geert Grooteplein 21, NL-6525 EZ Nijmegen, The Netherlands (E-mail: J.Goossens@science.ru.nl).

The costs of publication of this article were defrayed in part by the payment of page charges. The article must therefore be hereby marked "*advertisement*" in accordance with 18 U.S.C. Section 1734 solely to indicate this fact.

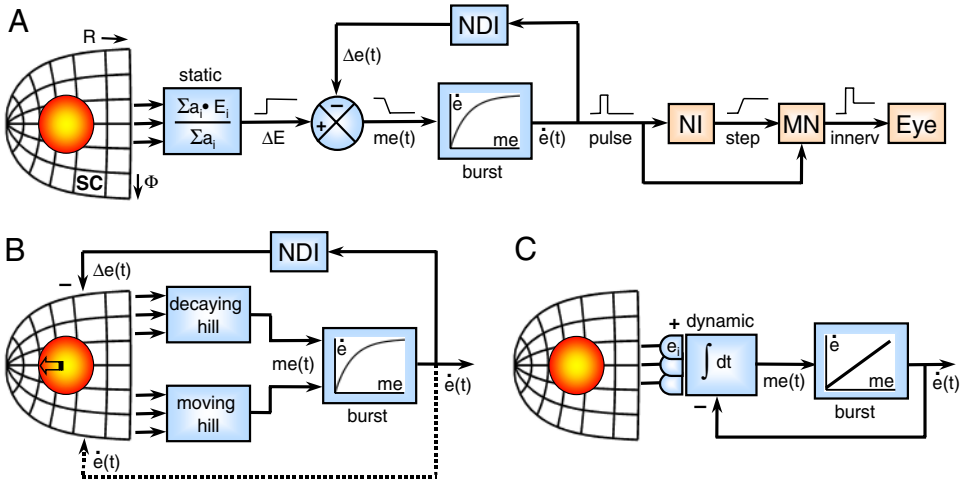

FIG. 1. Models of saccade generation. *A*: superior colliculus (SC) provides a static saccade goal (desired eye displacement) according to center of gravity of neural activity in its motor map. This spatial representation is decoded by (nonlinear) vector averaging of all cell contributions (a_i is the activity of cell i, and $\vec{E}_i$ is the saccade vector represented at each cell's location). Trajectory and kinematics of movement are controlled downstream by nonlinear local feedback. *B*: SC feedback models. "Decaying hill" model (Waitzman et al. 1991): eye displacement feedback inhibits population, such that instantaneous firing rate encodes dynamic motor error. "Moving hill" model (Munoz et al. 1991): eye velocity feedback (dashed) causes a caudal-to-rostral movement of population (arrow), location of which encodes dynamic motor error. Hybrid model (Wurtz and Optican 1994): both mechanisms operate through different SC subpopulations. *C*: in our new theory, SC population activity specifies an intended movement trajectory, which is decoded downstream by dynamic linear vector summation: each spike from a saccade-related SC neuron adds a fixed, site-specific vectorial contribution, $\vec{e}_i$ to movement command. Actual movement is controlled downstream by linear (rather than nonlinear) feedback. As in *B*, pulse-step innervation of eye plant is not shown; it is identical to that in *A* (red). ΔE, desired eye displacement; $\Delta e(t)$, current eye displacement; $me(t)$, dynamic motor error; $\dot{e}(t)$, current eye velocity; $\int dt$, temporal integration; Burst, brain stem burst generator; NI, neural eye position integrator; NDI, resettable neural eye displacement integrator; MN, motor neurons; innerv., eye plant pulse-step innervation signal.

Subsequent perturbation experiments have cast some doubt on the various SC feedback theories, because it appeared that SC activity does not quantitatively encode dynamic motor error (Goossens and Van Opstal 2000a,b; Keller and Edelman 1994; Munoz et al. 1996; Soetedjo et al. 2002a,b). Yet, the changes in burst activity that were observed in these experiments strengthen the notion that the SC output reflects a dynamic rather than a static movement command. However, controversy remains about how the spatial-temporal activity patterns in the SC are transformed into appropriate commands for the brain stem saccade generator (Anderson et al. 1998; Arai and Keller 2005; Guitton et al. 2003; Keller and Edelman 1994; Keller et al. 2000; Matsuo et al. 2004; Munoz et al. 1996; Port and Wurtz 2003; Port et al. 2000; Quaia et al. 1999; Scudder et al. 2002; Soetedjo et al. 2002a,b; Walton et al. 2005). One reason for this controversy is that most studies have related SC activity to straight saccades with little variability and near-normal kinematics. The large intertrial variability in a cell's saccade-related burst may then completely mask its relation with saccadic eye velocity, whereas this relation becomes quite clear when perturbations increase the variability in saccade kinematics (Goossens and Van Opstal 2000b; Soetedjo et al. 2002a).

Another problem is the lack of consensus about how to quantify the cell saccade-related bursts. A wide range of measures is in use. Movement fields, for example, have been described in terms of the number of spikes in the burst (Goossens and Van Opstal 2000b; Munoz and Wurtz 1995a), of the mean firing rate in either a fixed or a saccade-duration dependent time window (Edelman and Keller 1998; Ottes et al. 1986; Van Opstal and Van Gisbergen 1990), or of the peak firing rate that is estimated from a smoothed representation of the cell's instantaneous discharge (spike density functions; Port and Wurtz 2003).

Previously, we studied SC responses during blink-perturbed saccades (Goossens and Van Opstal 2000a,b). Blinks change many aspects of saccadic behavior and neural activity that include eye velocity, saccade duration and 2D trajectories, as well as the mean and peak firing rates and burst duration of SC cells. However, neither the blink-induced curvature of the eye movement, nor the subsequent compensatory phase to reach the target was reflected in the cells' discharge patterns. Interestingly, only the accuracy of the perturbed saccades and the number of spikes in the SC burst associated with these saccades remained unaffected. Very similar results have been obtained for straight saccades having perturbed kinematics in head-fixed monkeys (Munoz et al. 1996; Soetedjo et al. 2002b) and head-free cats (Matsuo et al. 2004). These latter results have received little attention thus far, but as we will argue in this study, they may be crucial for understanding the role of the SC in saccade generation.

New theoretical framework

In this study, we propose and test a new dynamic ensemble-coding model of the SC (Fig. 1*C*), which assumes that during the saccade each spike from a SC neuron simply adds a site-specific minivector to the intended eye displacement command. According to this idea, the SC output is a dynamic (rather than a static) signal, which represents the intended (rather than the actual) saccade trajectory. In our scheme, the brain stem decodes the dynamic SC output by linear vector summation (rather than by vector averaging) of the fixed movement tendencies provided by each spike and by linear decomposition into the appropriate horizontal and vertical eye displacement commands.

As we will explain in the results, this simple theory makes two important predictions. First, there should be an invariant,

monotonic relation between the instantaneous cumulative number of spikes in the cell bursts and the current eye displacement along the intended straight trajectory. Second, saccade-related SC cells should have dynamic movement fields that relate the cumulative number of spikes in the burst to the ongoing eye displacement, regardless the movement kinematics. This dynamic description can be obtained from the classic, static movement field (Ottes et al. 1986) without the need of additional tuning parameters. Because of the stereotyped kinematics of normal saccades, we have tested these predictions in detail using control and perturbed responses in the blink-perturbation paradigm.We also used measured activities of a large number of saccade-related SC cells to drive a linear 2D model of the brain stem to test whether dynamic linear vector summation can be used to decode the actual SC population activity for saccades to a single target. Interestingly, these simulations reveal a number of emerging properties of our theory that earlier saccade models had to incorporate explicitly: *1*) stretching of horizontal and vertical saccade components, *2*) straight trajectories, and most importantly, *3*) the nonlinear main sequence behavior of saccades. We therefore conjecture that the SC acts as a nonlinear vectorial pulse generator.

Finally, with the additional assumption that the saccade offset is determined by a fixed total spike count criterion, our conceptual scheme can also explain the effects of small reversible SC lesions (Lee et al. 1988).

METHODS

All experimental procedures were in accordance with the European Communities Council Directive of November 24 1986 (86/609/EEC), and were approved by the local university ethics committee. The data described here were collected from four rhesus monkeys (*Macaca mulatta*) that had been trained to refixate a small visual target with saccadic eye movements. Details about the setup, surgical procedures, and behavioral paradigms were described previously (Goossens and Van Opstal 2000a,b). Briefly, the animals were seated in a primate chair facing a spherical array of light-emitting diodes (LEDs) in an otherwise completely dark room. The head was restrained, and movements of the eye and eyelid were measured with the magnetic induction technique. Single cell recordings were made through an implanted recording cylinder using tungsten microelectrodes that were advanced into the SC by a hydraulic stepping motor.

We recorded in the intermediate and deep layers, at ~0.5–3 mm below the dorsal surface of the SC. The activity of 139 saccade-related SC neurons was studied with the use of a standard saccade task in which the animal made visually guided saccades from an initial fixation point to a peripheral target. The movement field of each neuron was characterized in detail by eliciting saccades to targets inside and neighboring the cell response field ("movement field scan"; resolution down to 0.5°). In addition, saccades were evoked to a fixed series of targets across the visual field (R between 2 and 35°, $\Phi \in$ [0,30, . . . 360]; "rose scan") to collect data for a fixed set of saccade vectors for each neuron. The responses of 25 neurons were examined further using the blink-perturbation paradigm. In this paradigm, saccades were made in complete darkness toward the remembered location of a visual target that was briefly (50 ms) flashed in the movement field of the cell. Air puffs (20 ms, 1.4–1.8 Bar) were presented in 30% of the trials to elicit a blink near saccade onset. In this way, saccades could be heavily perturbed by natural, noninvasive stimulation (Goossens and Van Opstal 2000a,b). Note that visual feedback was excluded in this case. Part of the data collected from these 25 cells was used in our previous study (Goossens and Van Opstal 2000b).

Data analysis

Saccades were detected off-line on the basis of the calibrated eye position signals using custom software (Goossens and Van Opstal 2000a). Spike trains recorded in each trial were represented as a sequence of δ pulses at the time of spike occurrence, t_k: $S(t) = \Sigma_k \delta(t - t_k)$ (1-ms resolution). The cumulative number of spikes in each trial, $CS(t)$, was calculated by temporal integration of the raw spike trains, starting 20 ms before saccade onset. The raw single cell activity was displayed in peristimulus time histograms and spike rasters that were aligned on specific events such as target onset and the onset of a saccade.

Data from the blink-perturbation paradigm were sorted into control and perturbation trials (Goossens and Van Opstal 2000a,b). Perturbation trials were selected on the basis of the presence of an air puff–evoked blink shortly before or after saccade onset and a concomitant increase in saccade duration (i.e., $\geq$1.5 times the average duration of corresponding controls). Atypically slow movements were removed from the control data. Subsequent analyses of each cell response properties typically included >10 trials per condition, but in no case <5 trials per condition were used.

Given the vectorial displacement of the eye (amplitude R, direction Φ) in each trial, movements were expressed in the coordinates of this vector (see Fig. 4). Toward that end, the saccade trajectory $[H(t),V(t)]$ was rotated over the angle Φ (counterclockwise rotation taken positive)

$$\begin{cases} H'(t) = H(t)\cos(\Phi) - V(t)\sin(\Phi) \\ V'(t) = H(t)\sin(\Phi) + V(t)\cos(\Phi) \end{cases} \quad (1)$$

The new horizontal coordinate, H', now aligns with the saccade displacement vector, whereas the new vertical coordinate, V', is perpendicular to this vector. The $H'(t)$ component thus describes the straight-line eye displacement in the direction of the saccade vector

$$\Delta E(t) = H(t)\cos(\Phi) - V(t)\sin(\Phi) \quad (2)$$

Spike density functions, $SD(t)$, were computed only for illustrative purposes. In Figs. 2 and 4, these smoothed representations of the instantaneous firing rate were generated by substituting each spike with a Gaussian pulse (adaptive width), and summing all Gaussians (Waitzman et al. 1991).

In Fig. 4*C*, cumulative spike counts from each cell were first resampled as function of eye displacement (ΔE) on a trial-by-trial basis to account for the variability in saccade kinematics. The response curves were then averaged per condition and normalized with respect to the mean control response. For each cell, a fixed delay of Δt=20 ms was introduced between its activity and the eye movement.

In Fig. 5, slopes, α, and biases, β, of the regression lines, $CS(t - \Delta t) = \alpha \cdot \Delta E(t) + \beta$, were determined from least-squares fits on the data of individual responses (2-ms resolution) and averaged across all trials toward a given movement field location. Pearson's correlation (r) between the spike counts and instantaneous eye displacement in each data set was calculated from the pooled data of the individual trials.

Static movement fields

Data collected in the movement field scans were used to characterize the static movement field of each cell (see Fig. 7*A* for illustration). Toward that end, we determined the magnitude of each saccade-related burst by counting the total number of spikes in a time window that ranged from 20 ms before saccade onset until 20 ms before saccade offset. The burst magnitude, N_s, as function of saccade amplitude, R, and direction, Φ, was quantified using the complex-logarithmic movement field model of Ottes et al. (1986)

$$N_s(R,\Phi) = N_o \cdot \exp\left[-\frac{(u - u_o)^2 + (v - v_o)^2}{2\sigma_o^2} \right] \quad (3)$$

where the variables $[u,v]$ (in mm) are the Cartesian coordinates in the

SC motor map that correspond to the polar coordinates $[R,\Phi]$ (in °) of a particular saccade vector in visual space (see afferent mapping function in Supplemental Material)[1]. Parameters $[u_o,v_o]$ (in mm) are the SC coordinates of the cell optimum saccade vector $[R_o,\Phi_o]$ (in °) that define the center of the cell's 2D Gaussian activation profile. N_o is the number of spikes in the burst for the optimal saccade vector. σ_o (in mm) denotes the tuning width of the cell in SC coordinates.

A nonlinear optimization algorithm (Nelder-Mead simplex, Matlab version 6, The Mathworks) was used to fit the four free parameters, N_o, $[u_o,v_o]$, and σ_o, according to the least squares criterion. Pearson's correlation (r) between data and fit ranged between 0.70 and 0.98 across the population of all 139 recorded neurons, where each fit was based on 100–400 responses.

Reconstruction procedure

Data collected from all 139 cells during normal, visually guided saccades of all amplitudes and directions were stored in a database that contained a total of 21,305 responses. From this library of results, we first estimated the spatial-temporal discharge patterns in the SC that were associated with horizontal, vertical, and oblique saccades. To test the predictions and emerging properties of our dynamic-ensemble coding theory, the instantaneous SC activity patterns were fed into the linear feedback model of the brain stem to reconstruct the 2D trajectories and kinematics of the associated saccades (Fig. 6).

ESTIMATING THE SC ACTIVITY IN SPACE AND TIME. The procedure to estimate the dynamic population activity in the SC for a particular saccade vector $[R,\Phi]$ involved the following steps. First, the anatomical coordinates $[u_c,v_c]$ (in mm) of each recorded cell c in the SC motor map were determined from the center of its static movement field ($[u_o,v_o]$ in *Eq. 3*; Supplemental Material; Ottes et al. 1986). Subsequently, we searched our database of single-unit responses (movement field scans and rose scans) and selected the raw spike data of all cells for measured saccades that matched the movement vector $[R,\Phi]$ (amplitude within ±5%, direction within ±5°). For each moment in time, t (1-ms resolution), we then projected each cell's spikes directly onto its location in the SC motor map.

Because the recording sites were not uniformly distributed, the resulting maps of spike events were smoothed with a spatial Gaussian smoothing kernel and resampled to obtain evenly spaced maps (at 0.1-mm resolution) of the instantaneous SC firing rates. Toward that end, each recorded spike occurrence t_c at time t was replaced with a 2D Gaussian (width, $\omega = 0.1$ mm) centered at the location $[u_c,v_c]$ of cell c that fired that spike. The instantaneous firing rate, $f_i(t)$, at each SC coordinate i was computed as the spatial average of the contributions of all Gaussians at that location

$$f_i(t) = \frac{1}{\rho_i}\sum_{c=1}^{P} S_c(t)\,\exp\left[-\frac{(u_i-u_c)^2+(v_i-v_c)^2}{2\omega^2}\right] \quad (4)$$

where $S_c(t)$ are the recorded spike events from cell c (represented as a sequence of δ pulses) for the saccade $[R,\Phi]$. P is the number of recorded SC cells. ρ_i represents the density of cell sampling at each site i

$$\rho_i = \sum_{c=1}^{P} \exp\left[-\frac{(u_i-u_c)^2+(v_i-v_c)^2}{2\omega^2}\right] \quad (5)$$

which is a fixed, and therefore linear, constant that does not depend on the cell's activity.

Each substitute Gaussian was truncated at the boundary of the ipsilateral SC, and the remainder was mapped onto the contralateral SC (see Van Gisbergen et al. 1987 for procedure) to ensure accurate estimates of the population activity for oblique and vertical saccades. In addition, the up-down and left-right symmetry of the SC motor map was used to increase the density of cell sampling, yielding 556 locations of recorded and mirror-reflected cells in the two colliculi (see Fig. 6*A*). A similar procedure of reflecting recording sites has been used by Anderson et al. (1998). The mean nearest-neighbor distance between cells was 0.2 ± 0.1 mm, which is >2.5 times smaller than the average tuning width (0.5 mm) of the cells' static movement fields in SC coordinates (see Fig. 7*C*).

Note that this method estimates the dynamic population activity directly from the cells' spike events associated with measured saccades of a particular amplitude and direction. This contrasts with previous studies (Anderson et al. 1998; Munoz and Wurtz 1995b) that first calculated spike density functions to estimate smoothed surface fits of each cell's dynamic activity for a range of saccades, which were used in turn to estimate each cell response for a particular saccade $[R,\Phi]$. Those fit results, rather than the cells' raw spike data, were subsequently projected onto the SC motor map and used to compute smoothed 2D representations of the SC firing rates at each moment in time.

Note also that our procedure does not make any assumptions about the distribution of activity on the SC motor map. If the activity would move across the map, either as a whole or within a subpopulation of cells, such changes would readily emerge from the reconstruction.

RECONSTRUCTING SACCADES FROM SC POPULATION ACTIVITY. In our model (Fig. 6), each spike from a neuron at site i produced a fixed minivector contribution, $\vec{e}_i$, according to its connection strengths to the brain stem. Specifically, the contribution of each spike from cell i to the horizontal ($e_{i,x}$) and vertical ($e_{i,y}$) premotor systems depended on the location $[u_i,v_i]$ of the cell in the SC according to the efferent mapping function, $[H(u_i,v_i),V(u_i,v_i)]$ (Van Gisbergen and Van Opstal 1989; Van Gisbergen et al. 1987; see Supplemental Material)

$$\begin{cases} e_{i,x} = \gamma_x \cdot H(u_i, v_i) \\ e_{i,y} = \gamma_y \cdot V(u_i, v_i) \end{cases} \quad (6)$$

where the two free parameters γ_x and γ_y are fixed scaling constants that were identical for all cells and all reconstructions. Linear vector summation of the movement contributions from all sites $i = 1,2,\ldots,M$ (0.1 × 0.1-mm resolution) at each point in time, t, yielded horizontal and vertical eye velocity signals

$$\begin{cases} \dot{E}_x(t) = \sum_{i=1}^{M} e_{i,x} \cdot f_i(t-\tau) \\ \dot{E}_y(t) = \sum_{i=1}^{M} e_{i,y} \cdot f_i(t-\tau) \end{cases} \quad (7)$$

where the free parameter τ is a fixed delay (identical for all cells) between the instantaneous firing rate $f_i(t)$ at site i (estimated by *Eq. 4*) and the ensuing events in the brain stem. Note that, given the fixed efferent connections of the SC cells with the brain stem, the amplitude and direction of the instantaneous eye velocity vector $[\dot{E}_x(t),\dot{E}_y(t)]$ depends entirely on the actual distribution of SC activity at each moment in time.

The eye velocity signals were calculated from saccade onset to saccade offset (2-ms resolution) and fed into a linear feedback model of the brain stem to reconstruct the 2D saccade trajectory and its kinematics (Fig. 6). The forward gain, B, and the feedback delay, d, were taken identical for the horizontal and vertical burst generators and served as the two remaining free parameters of the model in Fig. 6*A*. The best-fit values (least squares criterion) of the five model parameters γ_x, γ_y, τ, B, and d were found by fitting (Nelder-Mead simplex method, Matlab version 6, The Mathworks) the reconstructed 2D eye displacement and eye velocity profiles to the (average) measured profiles of nine different saccades distributed evenly across the oculomotor range.

[1]The Supplementary Material for this article is available online at http://jn.physiology.org/cgi/content/full/00889.2005/DC1.

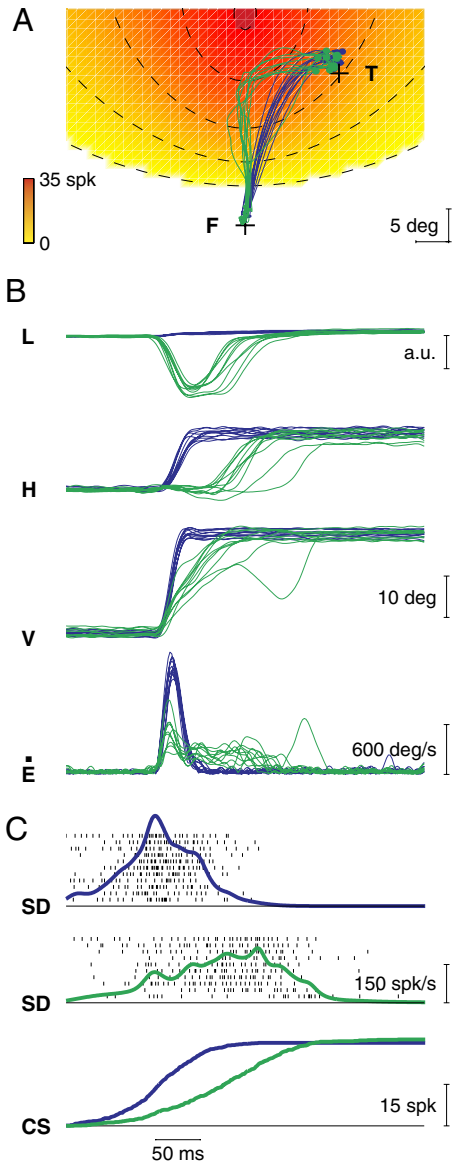

FIG. 2. Discharge of SC neuron pj4205 for control and blink-perturbed saccades. *A*: 2-dimensional (2D) trajectories of control (blue) and perturbed (green) saccades from the fixation spot (F) toward a flashed target (T) at $[R,\Phi]$ = [27,60]° in the cell's response field (color code; optimum at $[R_o,\Phi_o]$ = [35,90]°). *B*: time traces of eyelid position [$L(t)$; a.u., arbitrary units], eye position [$H(t)$, horizontal; $V(t)$, vertical], and track velocity [$\dot{E}(t)$] for control (blue) and perturbation (green) trials. Movements are aligned with saccade onset. *C*: spike rasters of neuron firing in control trials (*top*) and perturbation trials (*bottom*). Each row corresponds to a trial. Averaged spike density functions, $SD(t)$, are superimposed. $CS(t)$, cumulative number of spikes for control (blue) and perturbation (green) trials. Responses are aligned with saccade onset.

RESULTS

To test our dynamic vector-summation hypothesis (Fig. 1*C*), we collected data from 139 neurons within the SCs of four monkeys that showed an increase in their firing rate slightly before and tightly linked to the onset of saccades toward a particular region of the visual field (the movement field of the cell). We refer to these cells as saccade-related neurons or 'SC neurons' for short. A subset of 25 neurons was tested in the blink-perturbation paradigm. In our previous analysis of those cells (Goossens and Van Opstal 2000b), we quantified only the responses for saccades into the center of the cell movement fields, which constituted ~20% of the data set. In this study, we analyzed the responses in more detail and consider also the responses for saccades into different parts of the cell movement fields. We include these data because they offer an additional critical test of our theory.

Blink-perturbation paradigm

To explain the rationale of the analysis below, Fig. 2 provides a brief overview of the response patterns observed in the blink-perturbation paradigm by comparing the discharge of a typical SC neuron for control saccades (blue) and blink-perturbed saccades (green) toward a target in its movement field (color code). Note that the evoked blinks gave rise to strongly curved trajectories (Fig. 2*A*), a marked decrease and variability in saccade velocity, and a corresponding increase in saccade duration (Fig. 2*B*). Midflight compensation ensured, however, that the eye reached the target in total darkness. The burst activity of the cell underwent two major changes (Fig. 2*C*). First, the firing rate, for illustrative purposes represented here by spike density functions (SD), was reduced considerably. Second, the burst duration was increased and roughly matched the increase in saccade duration. Even so, the number of spikes for perturbed saccades (green trace) remained remarkably similar to that for control saccades (blue trace), as may be inferred from the cumulative number of spikes (CS) as function of time.

The often transient decreases in firing rate were temporally linked to the air puff onset (latency ~10 ms) and were also observed when air puffs were presented during the cell prelude activity (Goossens and Van Opstal 2000b). As shown in Fig. 3, we think this indicates that trigeminal reflex mechanisms somehow inhibit SC activity. The increases in burst duration could suggest that the SC contributes to the compensation for the blink-induced perturbations. However, our earlier analysis of the correlation between SC activity and the 2D saccade trajectory showed that neither the blink-induced curvature of the eye movement nor the subsequent compensatory phase to reach the target is reflected in the cell discharge patterns (Goossens and Van Opstal 2000b). Note, for example, that in Fig. 2, the compensation for the trajectory perturbation requires rightward movements of the eye and that the neuron cannot contribute to these movements because its movement field is upward and does not include rightward saccades. The intended movement (FT), on the other hand, is a straight saccade that falls well within the cell′s movement field. Moreover, the actual curved movements can be described behaviorally as the resultant of two superimposed movements: *1*) a slow but straight goal-directed saccade and *2*) a pure blink-related eye movement (Goossens and Van Opstal 2000a). We proposed that this superposition may occur at the level of the brain stem saccade generator because burst cells in the pontine reticular formation that fire for saccades are also active for blink-related eye movements (Cohen and Henn 1972), whereas SC cells do not fire for the latter movements (Goossens and Van Opstal 2000b). As depicted in the conceptual scheme of Fig. 3, these findings together suggest that the cells' prolonged activities reflect only the intended straight eye displacement trajectory rather than the actual curved movement.

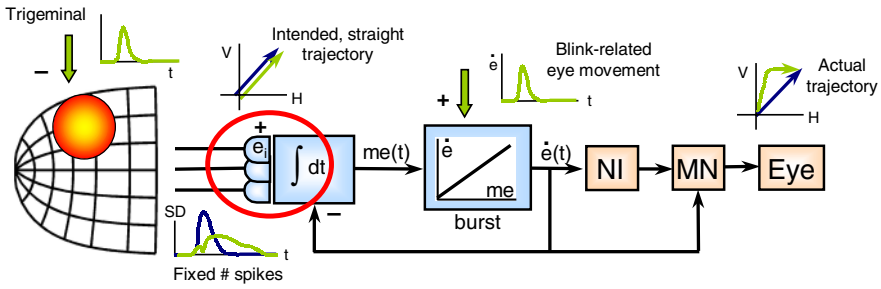

FIG. 3. Conceptual scheme of saccade-blink interactions. During blink-perturbations (green), firing rates in the SC (SD functions) are transiently suppressed by trigeminal or other blink-related inputs, but these changes do not reflect the actual 2D trajectory perturbations. Our hypothesis therefore entails that localized SC activity specifies only intended straight eye-displacement trajectory, through dynamic linear vector summation (occurring at processing stage within red ellipse). In this way, blink-induced decrease in SC firing rates results in a slow but straight eye displacement command. Actual curved trajectory results from superposition of this dynamic saccade command and a pure blink-related eye movement signal at a downstream level. Modified from Fig. 18 of Goossens and Van Opstal (2000b) to accommodate ensemble-coding theory. See Figs. 1 and 2 for abbreviations.

Spike train dynamics: evidence for vector summation

According to our linear ensemble-coding theory, the intended displacement of the eye as a function of time, t, is determined by linear addition of the movement contributions provided by all spikes, $k = [1,2, \ldots N_i(t)]$, from all saccade-related cells, $i = [1,2, \ldots M]$, in the SC motor map

$$\Delta\vec{E}(t) = \sum_{i=1}^{M}\sum_{k=1}^{N_i(t)} \vec{e}_i \cdot \delta(t - t_{i,k}) \qquad (8)$$

where $\vec{e}_i$ is the fixed, site-specific minivector contribution provided by a single spike from SC neuron i. Note that this theory makes no assumptions about the distribution of SC activity associated with a particular saccade. Any given trajectory, $\Delta\vec{E}(t)$ could in principle result from a wide range of different activation patterns.

In case of a single visual target, however, the intended movement will be a straight eye displacement toward the stimulus, and a single population of saccade-related cells at the corresponding location in the SC motor map will be active. Our proposal predicts that, under such conditions, the cumulative number of spikes in the burst of an active cell should be linearly related to the amplitude of the instantaneous eye displacement in the direction of the system's intended saccade vector, regardless the saccade kinematics and the actual 2D movement trajectory. To test this prediction, we analyzed and compared the spike trains recorded from saccade-related SC cells during normal control saccades and during blink-perturbed saccades to single visual targets.

Figure 4, *A* and *B,* shows this analysis for the responses of a typical SC neuron, when the monkey made a saccade toward the center of its movement field during a control trial (blue) and a perturbation trial (green). From the raw data (Fig. 4*A*), we first calculated the instantaneous eye displacement, $\Delta E(t)$, along the optimal, straight saccade trajectory (dashed) by projecting the actual eye position coordinates $[H(t), V(t)]$ (Fig. $4A_2$) onto the straight line connecting the initial fixation point and final endpoint (Fig. $4B_1$; *Eqs. 1* and *2*). Subsequently, the cumulative number of spikes, $CS(t)$, was determined from 20 ms before saccade onset (Fig. $4B_1$). The spike count data were delayed by 20 ms and plotted as function of the (intended) eye displacement (Fig. $4B_2$). This 20-ms delay is based on the observation that the lead time of the saccade-related burst of SC cells relative to movement onset, as well as the latency of electrically evoked saccades, are in this range (Sparks and Hartwich-Young 1989; Van Opstal et al. 1990; Waitzman et al. 1991). Note that the resulting response curves for the control and perturbed saccade follow very similar and roughly linear trajectories (Fig. $4B_2$), whereas the temporal evolution of the spike count and eye displacement curves was considerably different for the two movements (Fig. $4B_1$). This result was also highly consistent across trials (dots). Thus the temporal discharge patterns of this cell reflected neither the curvature of the eye movement nor the subsequent compensatory phase, but were faithfully related to the intended straight (1D) eye displacement trajectory. Clearly, this is not just a consequence of a similar number of spikes in the burst or a consequence of the eye displacement and cumulative spike counts having monotonic time-courses. For example, a wide range of very different response curves were obtained when the cumulative spike counts from the control trials were plotted as function of the eye displacement in the perturbation trials and vice versa (see Supplemental Material; see also Figs. 5*A* and 8, *A* and *B*).

Figure 4*C* shows that comparable results were obtained for all 25 neurons that could be fully tested in the control (green) and perturbed (blue) condition. Although the response curves (thin; averaged across trials) of the individual cells were not always fully identical between the two conditions, the population average of the responses in the blinking condition matches the average control curve very closely (thick; no significant differences; t-test, $P > 0.13$). Thus in line with the predictions of *Eq. 8*, the cumulative number of spikes in the SC burst, delayed by about 20 ms relative to saccade onset, provides a good descriptor of the instantaneous displacement of the eye along its intended straight trajectory, regardless the saccade kinematics and regardless the actual 2D movement trajectory.

For each neuron, we further quantified these dynamic response relations for saccades into different parts of the movement field using linear regression. Figure 5*A* exemplifies this analysis for a typical SC neuron, when the monkey made saccades to five different target locations (1–5). Note that in all five cases, there is a tight, near-linear relation between the cell's cumulative spike count and the instantaneous eye displacement, and that the data for straight, high-velocity control saccades (blue) and curved, low-velocity perturbed saccades (green) yield very similar regression lines (solid). Moreover, the response curves reach an almost fixed spike count value, which is systematically different for each saccade vector according to the cell's movement field properties. For example,

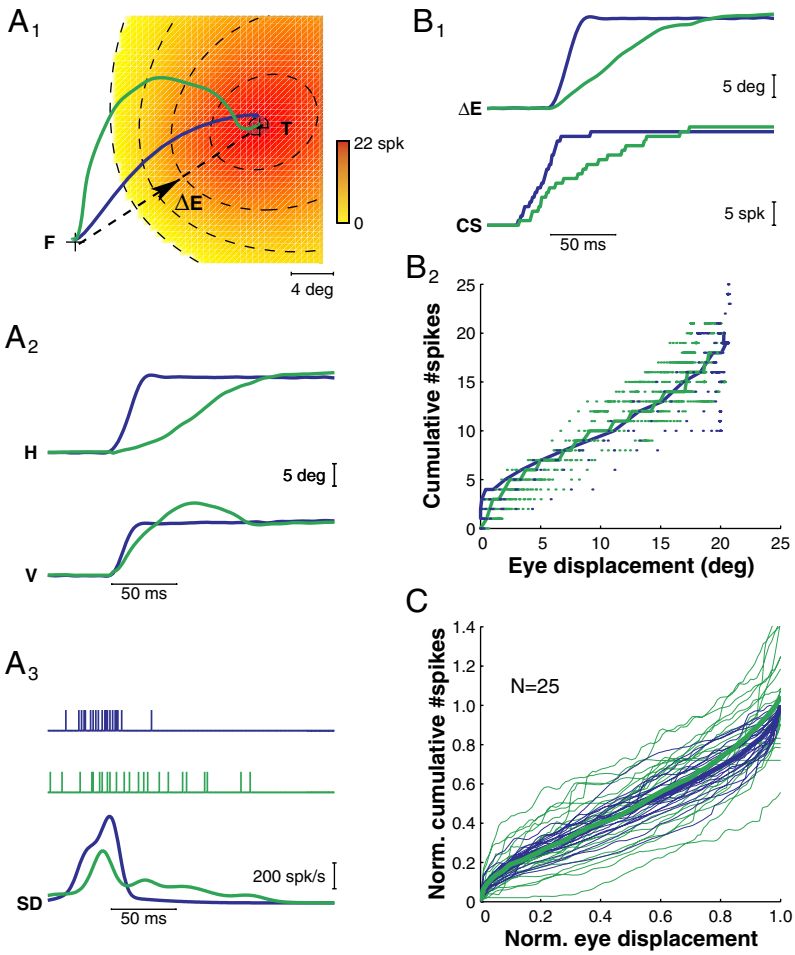

FIG. 4. Cumulative number of spikes reflects current eye displacement. *A*: raw data from a representative control trial (blue) and perturbation trial (green) to center of movement field of cell pj5202. Dotted line (FT) represents the straight, intended eye displacement, ΔE. Movement field (color code) is only shown for illustrative purposes. B_1: component amplitude of eye displacement along FT, $\Delta E(t)$, and cumulative number of spikes, $CS(t)$, as function of time for both movements. B_2: cumulative spike counts as function of intended eye displacement for control and perturbed response. Dots are data from additional control ($n = 7$) and perturbation ($n = 12$) trials. *C*: averaged and normalized response curves for control (blue) and perturbed (green) saccades toward movement field center for all 25 neurons tested in this way. Population response (thick) for the 2 conditions is very similar.

the burst for control and perturbed saccades toward the center of the movement field in Fig. $5A_2$ contained ~23 spikes, whereas this number dropped to ~10 spikes for the control and perturbed saccades in Fig. $5A_5$. This difference across saccade vectors is also reflected in the slopes, α, of the regression lines. The slopes of the two regression lines in Fig. $5A_2$, for instance, are much steeper than the ones in Fig. $5A_5$, because the movement vectors in Fig. $5A_2$ are closer to the neuron's preferred vector. Note, however, that the slopes are not simply determined by the number of spikes in the burst. For example, the burst for control and perturbed saccades in Fig. 5, A_1 and A_3, contained ~18 spikes, but the slopes of the two regression lines in Fig. $5A_1$ are much steeper than the ones in Fig. $5A_3$. The data thus show that the number of spikes per degree eye displacement that this cell fired during a saccade depended systematically on the system's intended movement vector and that the cell's dynamic activity faithfully reflected the actual movement kinematics along that vector.

The scatter plots in Fig. 5, *B* and *C,* summarize the regression results for all 25 neurons tested in this way. As predicted by *Eq. 8*, there was a strong correlation between the cumulative number of spikes and the instantaneous eye displacement for the cells' preferred vector (●), for less optimal vectors (○), and for both experimental conditions (Fig. 5*B*; mean correlation, $r = 0.79 \pm 0.13$ and $r = 0.76 \pm 0.15$ for control and perturbed conditions, respectively). In addition, the slopes of the regression lines were very similar for control and perturbed responses (Fig. 5*C*), despite considerable differences in the kinematics and 2D trajectories of the associated saccades. The mean difference across all data sets was not statistically significant (*t*-test, $P > 0.05$). For responses toward the center of the cells' movement fields (●), the difference between the two conditions was on average only $7 \pm 7\%$ (*t*-test, $P = 0.04$) and not significantly different from zero for most individual cells (17/25; *t*-test, $P > 0.05$).

Reading the population code

Figures 4 and 5 show a clear link between the detailed spike patterns of the cell bursts and the kinematics of the eye displacement along the intended straight trajectory. However, the discharge of an individual SC neuron cannot unequivocally encode the intended trajectory because the relationship between the cumulative number of spikes in the cell's burst and the instantaneous eye displacement is different for each movement vector. Interestingly, however, this dynamic relationship depends systematically on the amplitude and direction of the saccade vector within a cell's movement field (Fig. 5*A*). This suggests that the eye movement command is a dynamic population signal based on vector summation of site-specific movement tendencies provided by all spikes from all recruited SC cells (*Eq. 8*). To test this idea quantitatively, we recorded from 139 saccade-related SC neurons throughout the SC motor map, and we applied the raw discharge patterns of these cells

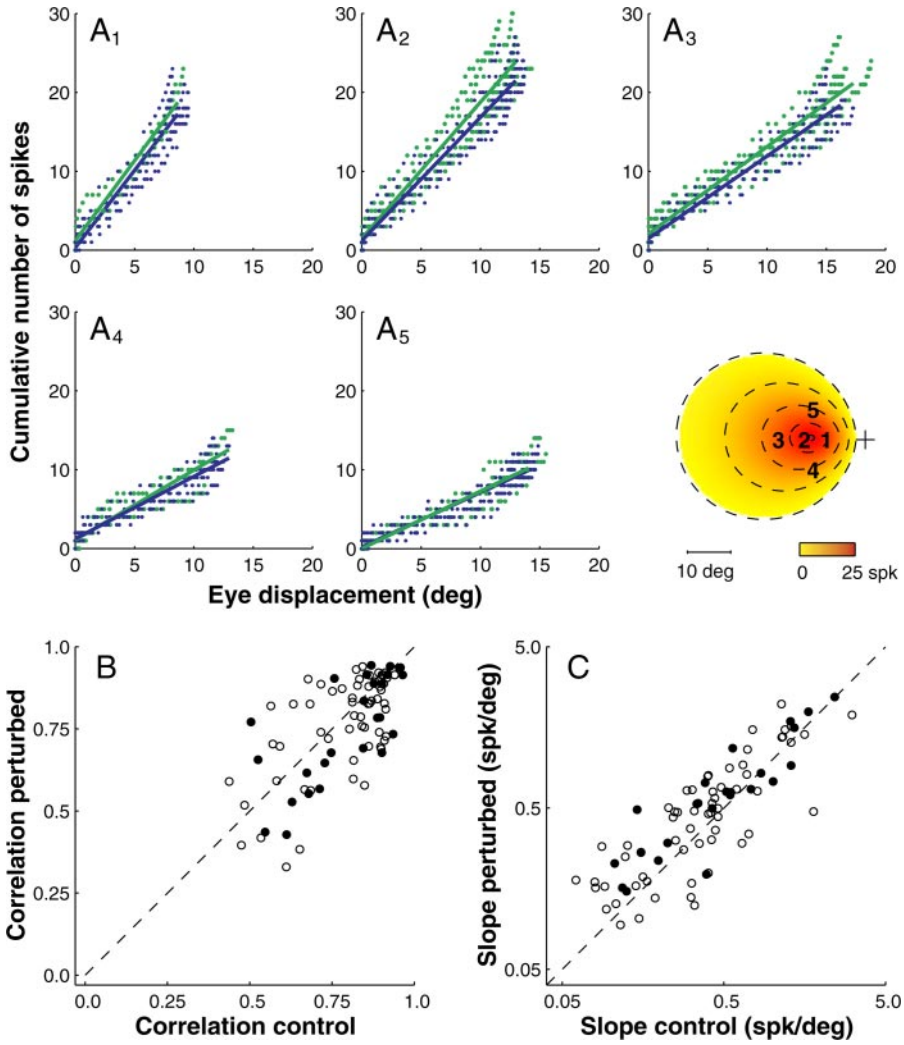

FIG. 5. Discharge dynamics across the movement field. A_1–A_5: cumulative spike count vs. eye displacement curves for control (blue) and perturbed (green) responses of SC neuron er0904 for saccades to 5 different locations (1–5) in its movement field. Dots, individual data samples; lines, linear regression results. Number of spikes in burst and slope, α, of regression lines depend systematically on system's intended movement vector according to cell's movement field. *B* and *C*: regression results for all 25 SC cells tested in the blink-perturbation paradigm. ●, results for saccades to movement field center; ○, saccades into peripheral movement field; dashed lines, identity lines. *B*: correlation (r) between spike counts and eye displacement is high under both experimental conditions. *C*: slopes are very similar for control and perturbed responses.

for normal visually guided saccades to a linear, 2D saccade model of the brain stem (Fig. 6*A*; see METHODS for details). Inspired by Scudder's original 1D model (Scudder 1988), this new model assumes a spatial-temporal integration stage at the comparator rather than resettable integrators in the feedback loop.

In short, we first determined the anatomic location of each neuron in the SC motor map from its optimal saccade vector (Ottes et al. 1986). We then estimated the dynamic SC activity associated with a particular saccade vector from the cell responses recorded during saccades of that particular amplitude and direction. Toward that end, we mapped each cell's spikes directly onto its location in the SC motor map, and from the measured spike events at each recording site, we calculated spatially (not temporally) smoothed maps of the instantaneous firing rates. The resulting estimates of the SC firing patterns in space and time were subsequently decomposed into dynamic horizontal and vertical movement commands. In line with neuroanatomical data (Chimoto et al. 1996; Moschovakis et al. 1998; Scudder et al. 1996), we used the efferent mapping function (Van Gisbergen and Van Opstal 1989; Van Gisbergen et al. 1987) that assumes that SC neurons excite horizontal and vertical burst neurons in the brain stem with weights that are a function of their position in the SC motor map. The scheme in Fig. 6*A* thus represents a "multiple-source" model in which each individual SC cell provides an independent dynamic contribution to the brain stem. The brain stem circuit for the horizontal and vertical eye movement components was modeled by two independent linear feedback systems, which is consistent with recent lesion experiments in the paramedian pontine reticular formation (Barton et al. 2003). Only five parameters had to be optimized: a fixed delay (identical for all cells) between SC and brain stem activation, two scaling factors, γ_x and γ_y (identical for all cells), that scaled the site-specific horizontal and vertical SC projection strengths to the brain stem, the feedforward gain, *B*, of the brain stem pulse generators, and a fixed delay in the local feedback loops. The best-fit values of these parameters (Fig. 6) were determined from a subset of nine different responses. In all subsequent reconstructions, the parameters of the brain stem model were kept fixed.

Figure 6*B* shows the measured SC activity patterns for a rightward horizontal saccade toward a single visual target at $[R,\Phi] = [21,0]^\circ$, together with the eye movement that was reconstructed from these activity patterns. Note that cells in a restricted region of the SC were recruited and that this "mountain" of activity stays at the same motor map location during the saccade (*insets*). Furthermore, the reconstruction (green) generated a realistic saccadic profile that closely matched the (average) measured saccade (blue). Cells at different locations in the SC motor map were active for small and large saccades and for saccades in different directions. Figure 6*C* shows that

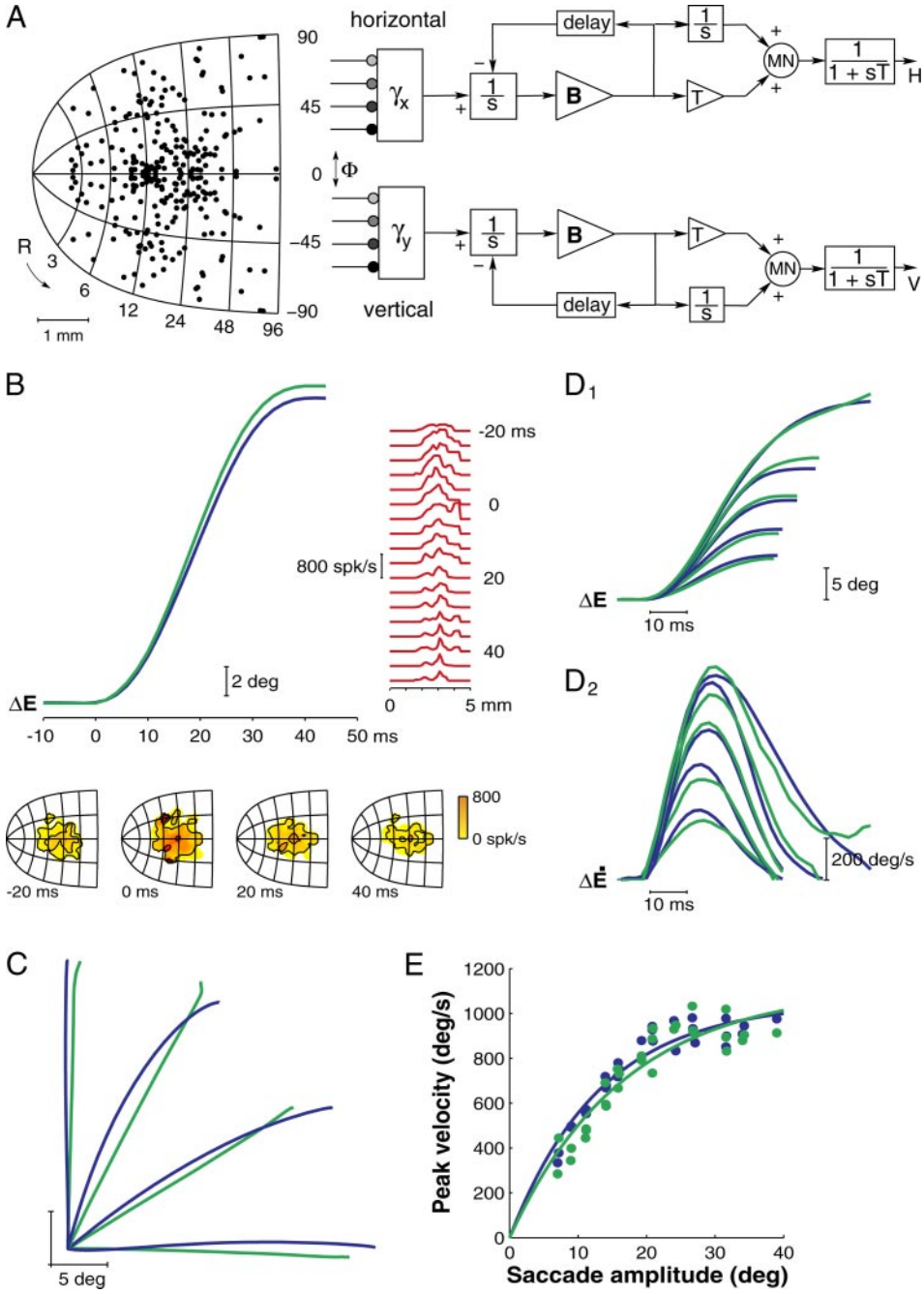

FIG. 6. Saccade reconstruction from measured SC activity. *A*: linear 2D model of SC-brain stem saccade generator. Locations of recorded and mirror-reflected cells are indicated on SC motor map (●). R and Φ (in °): polar coordinates superimposed on the motor map. Parameters: $\gamma_x = 9.1 \times 10^{-7}$ and $\gamma_y = 8.5 \times 10^{-7}$, scaling factors of SC projection strengths to brain stem; $B = 86$ spikes/s/°, forward gain of burst generators; delay = 8 ms, delay in local feedback loop; $T = 150$ ms, time constant of 1st-order eye plant; 1/s, neural integration (Laplace notation). SC activity reached the brain stem after $\tau = 10$ ms. *B*: measured (blue) and reconstructed (green) horizontal saccades ($[R,\Phi] = [21,0]°$). *Insets*: maps of instantaneous firing rates, $f_i(t)$, in the contralateral SC (*bottom*) and distribution of activity along rostral-to-caudal axis (*left*; 0 mm corresponds to rostral pole) at different moments in time, starting 20 ms before saccade onset. Activity maps were calculated directly from raw spike data by mapping spike events associated with measured saccades $[R,\Phi] \approx [21,0]°$ onto each cell's location in the motor map. No dynamic movement field fits were used. *C*: 2D trajectories of reconstructed and measured saccades in oblique directions were approximately straight. *D*: reconstructions produced realistic eye displacement [$\Delta E(t)$; D_1] and eye velocity [$\Delta \dot{E}(t)$; D_2] profiles for saccades of different amplitudes ($R = [7,11,16,21,32]°$; $\Phi = 30°$). *E*: model (green) reproduces nonlinear amplitude-peak velocity relationship of normal saccades (blue).

the reconstructions of the eye movements associated with these different discharge patterns yielded approximately straight trajectories, not only for horizontal and vertical saccades, but also for oblique saccades. One should realize that the scheme in Fig. 6 does not assume the planning of a straight saccade; it is a multiple source model with independent horizontal and vertical burst generators. The only "straight" contribution to the movement is the tiny vectorial displacement provided by a single spike fired by a single cell. Even so, in the reconstructions, the horizontal and vertical saccade components show the correct amount of "stretching" that is needed to obtain straight oblique saccades. Thus straight saccades are an emerging property of the model that results entirely from the actual spatial-temporal discharge patterns in the SC motor map. Figure 6*D* shows that the position traces and velocity profiles of saccades with different amplitudes are predicted quite well by this simple model. For example, the reconstructions reproduced both the bell-shaped velocity profiles of small saccades and the skewed velocity profiles of large saccades (Fig. 6D_2). Accordingly, the amplitude-peak velocity relation ("main sequence") for reconstructed saccades (green) and measured (blue) saccades is virtually identical (Fig. 6*E*). Fit parameters of the two exponential curves (Van Gisbergen et al. 1985) were not significantly different (*t*-test, $P > 0.2$). Note, however, that the brain stem circuit in the model is entirely linear. Hence, the dynamic nonlinearity in the saccadic system that is generally supposed to underlie the main sequence relation appears to be embedded in the measured SC activity patterns.

Static movement fields

Obviously, the spatial distribution of saccade-related SC activity depends on the properties of the collicular movement fields. Note, however, that the data analysis up to and including Fig. 6 has not incorporated the notion of a cell movement field. The movement field plots in Figs. 4 and 5 only served to delineate the range of saccade vectors for which the cells fired, and for the analysis in Fig. 6, we only used each cell preferred vector to estimate its location in the motor map.

In Fig. 7, we quantified the classical, static movement fields of all 139 cells. As shown in Fig. 7*A* for one of the cells, we described the total number of spikes in the burst, N_s, as function of saccade amplitude, R, and direction, Φ, using the complex-logarithmic movement field model of Ottes et al. (1986). For clarity, we highlighted the results for a cross-section in amplitude (green) and direction (blue). As one may recall from Figs. 2 and 4, the total number of spikes in the burst is invariant to spatial-temporal perturbations of the saccade trajectory, which means that this quantity is a reliable measure to describe a cell's static movement field, unlike the mean and peak firing rate in the burst that do not exhibit a fixed relation to saccade amplitude and direction.

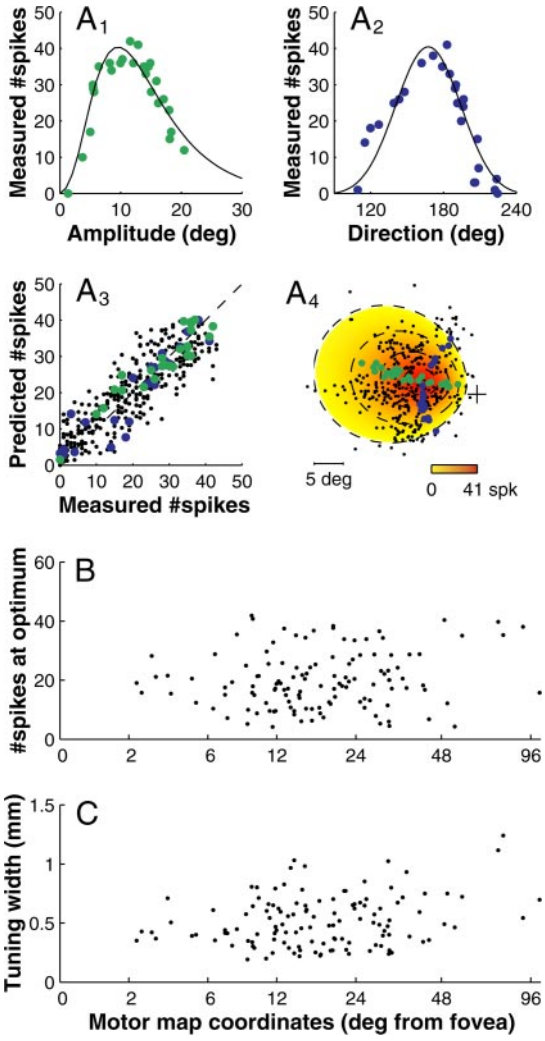

FIG. 7. Static movement fields. *A*: static movement field (Ottes et al. 1986) of cell er0902. A_1 and A_2: number of spikes in burst, N_s, for saccades whose directions or amplitudes matched either optimal direction (A_1; green, $n = 25$) or optimal amplitude (A_2; blue, $n = 26$) of the cell's preferred vector ($[R_o,\Phi_o] = [9.5,167]°$). Movement vectors (●) are superimposed on fitted 2D movement field representation (color code; A_4). Note good correspondence between data and model (A_3; $r = 0.92$; $n = 326$ responses). *B*: number of spikes in burst of each cell for its preferred saccade vector, N_o, as a function of its location in the SC motor map, for all 139 tested cells. *C*: tuning width, σ_o, of all 139 cells as function of their location in the motor map.

In Fig. 7*B,* we plotted the number of spikes in the burst of each cell for its preferred vector as a function of its estimated location in the SC motor map. In line with earlier studies (Munoz and Wurtz 1995a; Van Opstal and Hepp 1995), we found no systematic relation between the number of spikes at the optimal vector and the cell's motor map coordinates ($r = 0.1$, average value $N_o = 20 \pm 9$ spikes). In addition, we found no systematic relation between the cell's motor map coordinates and the width of their static movement fields ($r = 0.1$, average value $\sigma_o = 0.5 \pm 0.2$ mm; Fig. 7*C*). Figure 7, *B* and *C,* thus indicates that, for different saccade vectors, the magnitude and spatial extent of the SC activation profile (expressed in numbers of spikes) is about the same. Assuming a uniform cell density across the SC motor map, these results therefore suggest that the total number of spikes across the entire active population is invariant across the motor map. Thus for each particular saccade, the brain stem receives roughly the same number of spikes from the motor SC.

Dynamic movement fields

Figure 6 indicates that the straight trajectories and the nonlinear kinematics of normal saccades can be fully retrieved from the SC population activity based on the sole assumption that each SC spike adds a site-specific minivector to the dynamic eye displacement command (*Eq. 8*). Conversely, these findings suggest that when a straight saccade is planned (i.e., when a single, stationary population of cells is recruited), it is possible to predict the spike trains of each neuron for that saccade from the parameters of its static movement field. In fact, under these conditions, the dynamic vector-summation model predicts the following relationship between the cumulative number of spikes in the burst of a particular cell and the instantaneous eye displacement during any saccade

$$CS(t + \Delta t) = \frac{N_s(R,\Phi)}{R} \cdot \Delta E(t) \equiv \alpha(R,\Phi) \cdot \Delta E(t) \qquad (9)$$

where $N_s(R,\Phi)$ is the static movement field description (Ottes et al. 1986) of the cell that specifies the total number of spikes in the burst as function of saccade amplitude and direction. Δt is a fixed delay between the neural data and the ensuing eye movement. $\alpha(R,\Phi)$ is the slope of the cell′s dynamic response curve that is inversely proportional to the intended saccade vector (cf., Fig. 5) and that reflects the number of spikes per degree eye displacement that the cell will fire during that movement. Note, that a fixed delay is a slight simplification, because Sparks and Mays (1980) have shown that for saccades into the peripheral movement field, the onset of the cell bursts relative to saccade onset increases. We have not attempted to incorporate this detail in the present description.

Because quantitative predictions of the SC discharge dynamics have not been tested in earlier studies, we first analyzed the saccade-related responses of all 139 neurons for normal, visually guided saccades. Figure 8, *A–D,* shows this analysis for a typical cell (same neuron as in Fig. 7*A*). First we determined

the classical movement field, $N_s(R,\Phi)$, of the cell as shown in Fig. 7*A*. We then used this static movement field description to predict the measured discharge patterns of the cell for individual saccades into its movement field (*Eq. 9*, 2-ms resolution, $\Delta t = 20$ ms). Figure 8, *A* and *B,* shows the discharge dynamics of the cell for a subset of responses (same trials as in Fig. 7, A_1 and A_2). Note that the temporal evolution of the spike counts was different for each saccade vector (Fig. 8*A*) and that a wide range of response curves was obtained (Fig. 8*B*). In Fig. 8*C*, each of these response curves is predicted by *Eq. 9* and compared with the actual response curves by plotting the measured cumulative number of spikes for each saccade versus the predicted cumulative number of spikes for that saccade. Thus time and eye displacement are implicit in this plot. Note that the data nicely align with the diagonal line (dashed), indicating that the cumulative number of spikes in the cell burst is predicted quite well for all individual saccades (Fig. 8*C*), despite considerable variation in saccade metrics, kinematics, and spike counts (Fig. 8, *A* and *B*). Accordingly, the predicted slopes $\alpha(R,\Phi)$ of the response curves were in close agreement with the slopes of the measured response curves (cf. Fig. 8*B*) for all saccades into the cell's movement field (Fig. 8*D*).

Figure 8*E* summarizes the goodness-of-fit of the dynamic movement field model (*Eq. 9*) for all 139 neurons that we have tested in this way. For each cell, we calculated the correlation between the measured and predicted discharge patterns from the sampled data (2-ms resolution) of all visually guided responses into the cell movement field (typically, *n* between 50 and 250). The analysis thus included hundreds to thousands of data points per cell. Note that high correlations were obtained for the entire population of 139 neurons (population average, $r = 0.83 \pm 0.08$), indicating that the dynamic movement field model of *Eq. 9* provides a very good description of the neurons' temporal discharge patterns. This is quite remarkable given that the model of *Eq. 9* has only four free parameters (i.e., preferred saccade amplitude and direction, total number of spikes for the preferred displacement vector, and spatial tuning width in $N_s(R,\Phi)$; see *Eq. 3*), none of them having any explicit relation to the cell's discharge dynamics.

As an additional critical test of our theory, Fig. 9 also compares the dynamic movement field predictions to the measured responses of all 25 cells in the blink-perturbation paradigm. For these cells, the static movement fields were estimated from independent data collected during visually guided saccades (movement field scans). Still, the number of spikes in the burst (Fig. 9*A*) and the slopes $\alpha(R,\Phi)$ of *Eq. 9* (Fig. 9*B*) were predicted quite accurately for all memory-guided control responses (blue; $r = 0.92$ and $r = 0.96$, respectively). Even for the responses associated with heavily perturbed, slow, and curved saccades, both the predicted number of spikes and the predicted slopes corresponded closely to the actual data (green; $r = 0.87$ and $r = 0.80$, respectively). For most cells, the correlation between measured and predicted cumulative spike counts (2-ms resolution) across all saccades was quite high and roughly comparable for the two experimental conditions (Fig. 9*C*; population average, $r = 0.76 \pm 0.16$ and $r = 0.69 \pm 0.16$ for control and perturbed responses, respectively), despite

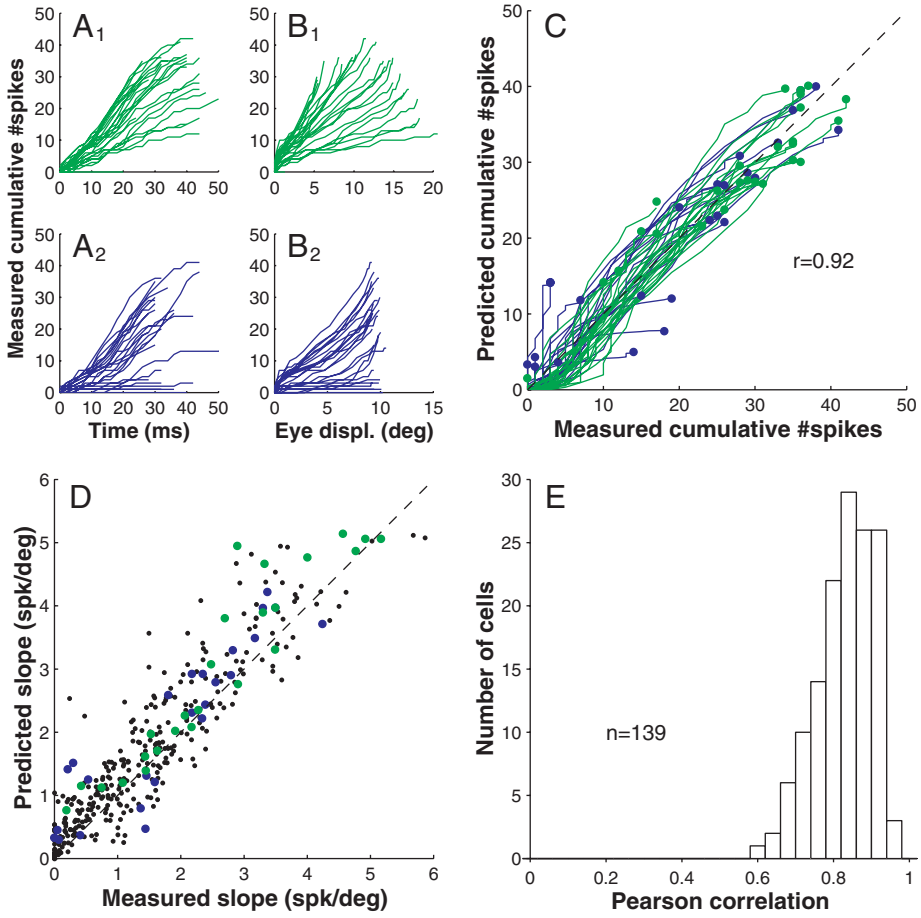

FIG. 8. Dynamic movement fields. *A* and *B*: measured discharge dynamics of cell er0902 from 20 ms before saccade onset until 20 ms before saccade offset. Saccades varied in amplitude (A_1 and B_1; green, $n = 25$) or direction (A_2 and B_2; blue, $n = 26$) as they did in Fig. 7, A_1 and A_2, respectively (same cell, same trials). Note considerable differences in spike count evolution as function of time (*A*) and of current eye displacement (*B*) for different saccade vectors. *C*: predicted (*Eq. 9*) vs. measured cumulative spike counts for responses in *A* and *B* align with identity line (dashed). Correlation $r = 0.92$ across $n = 9{,}472$ data samples from all 326 responses into the cell's movement field (cf. Fig. $7A_4$). *D*: slopes of spike count vs. eye displacement regression lines (cf. *B*) were predicted quite accurately ($r = 0.95$) for all $n = 326$ saccades into movement field. *E*: high correlations between sampled data and dynamic movement field model (*Eq. 9*, 2-ms resolution) were obtained for all 139 SC neurons tested with visually guided saccades (typically, *n* between 50 and 250) across their movement field.

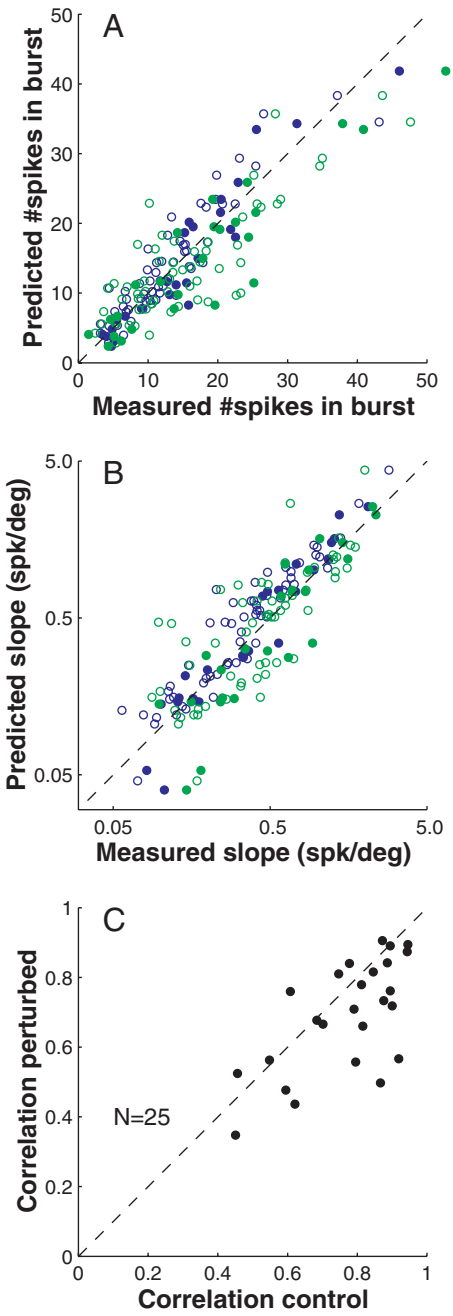

FIG. 9. Prediction of discharge dynamics in the blink-perturbation paradigm. *A* and *B*: number of spikes in burst (N_s; *A*) and slopes of response curves (α; *B*) are predicted remarkably well for control (blue) and perturbed (green) responses for all 25 cells. Responses toward the center (●) and to more peripheral (○) movement field locations (cf., Fig. 5*A*) are indicated. *C*: overall correlations between data and model predictions (*Eq. 9*; 2-ms resolution) were hardly affected by blink-evoked disturbances.

considerable differences in kinematics and 2D trajectories of the saccades (cf. Figs. 2 and 4).

DISCUSSION

In summary, we found that the cumulative number of spikes in the cell bursts correlates very well with the instantaneous displacement of the eye along the straight intended trajectory for both normal and strongly perturbed saccades (Fig. 4) and that this result applies to all saccades within a cell movement field (Fig. 5). These new findings suggest a neural population code that is based on dynamic vector summation (*Eq. 8*). We tested this new theory further by applying the spike data from a large population of SC neurons to a simple linear model of the brain stem (Fig. 6). Previous studies have never used measured spatial-temporal SC activity patterns to quantitatively test how the SC activity may be decoded into appropriate control signals for the eye muscles. The results showed that reconstructed saccades are straight in all directions (not built into the model) and have the correct nonlinear main sequence behavior (not built into the model). These remarkable findings led to the new insight (formalized in *Eq. 9*) that a cell's dynamic movement field can be fully described from its well-established static movement field, without the necessity for any additional parameters. When we evaluated this implication of the dynamic vector summation model, accurate predictions of the cell dynamic firing patterns were obtained for normal saccades (Figs. 8 and 9) as well as highly perturbed saccades (Fig. 9). Earlier population-coding models of the SC (Fig. 1, *A* and *B*) imply ambiguous movement field descriptions that depend on saccade kinematics and therefore have not been able to establish a quantitative link between the discharge dynamics of SC cells and their movement fields.

Our results indicate that the instantaneous SC activity for saccades to single visual targets represents straight trajectories and kinematics in the direction of the intended eye displacement vector. These results are nicely in line with electrical stimulation experiments, which always yield straight saccades in the preferred direction of the stimulated SC neurons, regardless the stimulation parameters used, whereas the amplitude and velocity of saccades evoked at a particular site can be systematically altered by manipulating the intensity, number, and frequency of the stimulation pulses (Stanford et al. 1996; Van Opstal et al. 1990). Classic models of the SC (Fig. 1*A*) predict that the movement kinematics are unrelated to the cell temporal discharge patterns because the population activity would only specify the coordinates of the saccade goal. Our study shows that the cumulative number of spikes in the saccade-related burst provides an invariant predictor for the saccadic movement, regardless of its kinematics (Figs. 2, 4, and 5). Better still, the dynamic movement field model of *Eq. 9* provides a full quantitative description of the cell instantaneous discharge patterns for both extremely slow and high-speed normal saccades (Figs. 8 and 9). We believe such findings are difficult to reconcile with the idea that activity in the SC motor map is not involved in motor control but reflects only the selection of a saccade goal (Krauzlis et al. 2004; Port and Wurtz 2003).

Normometric saccades

According to the scheme in Fig. 6, multiple factors will affect the amplitude and direction of a saccade: *1*) the size of the population, *2*) the distribution of activity within the population, *3*) the number of spikes of each individual cell, and *4*) the efferent connection strength of each cell with the brain stem. In our model, the latter was taken from Ottes et al. (1986), but the first three factors were not part of the model, because they were completely determined by the actually measured distribution of activity across the motor map. It is

therefore far from trivial that this simple scheme did indeed generate normometric saccades for all amplitudes and directions, while necessitating only two free tuning parameters for the horizontal and vertical saccade components, γ_x and γ_y in *Eq. 6*. In an earlier simulation study from this laboratory, we have shown that under the additional assumption, the population activity can be described by a translation-invariant 2D Gaussian in the motor map, a linear vector summation projection scheme can indeed work (Van Gisbergen et al. 1987).

The fact that the new dynamic vector summation scheme of Fig. 6 generates straight, normometric saccades with the correct kinematics therefore suggests a precise tuning of the neural population in which the size, instantaneous distribution, and the total number of spikes are just right. Indeed, our analysis of the static movement field parameters (Fig. 7) shows that the 2D activation profile is roughly translation-invariant across the motor map, with a Gaussian width (σ) of ~0.5 mm (corresponding to a diameter of 2–3 mm), which agrees nicely with the model assumptions of Ottes et al. (1986) and Van Opstal and Hepp (1995). In addition, our results also suggest that the total number of spikes issued by the neural population in the saccade-related burst is roughly the same for different saccades across the motor map.

Feedback

Our data show a clear link between the detailed spike patterns of the SC burst and the ensuing eye movement events, but not that such is determined by eye movement feedback at the level of the SC. During the blink-perturbations, activity in the SC is transiently suppressed at extremely short latencies by trigeminal reflex mechanisms that are as yet not clear (see Fig. 3 and Goossens and Van Opstal 2000b for discussion). According to our simple scheme, the resulting decreases in SC firing rates are the root cause of the decreases in eye velocity, because in our scheme, the SC is commanding the eye movement (through its efferent projections to the oculomotor brain stem). The SC could receive some form of global feedback (e.g., about saccade duration, as was suggested by Soetedjo et al. 2002a), but SC cells do not need local feedback about the actual 2D trajectory of the eye to produce a fixed number of spikes (Fig. 10). Indeed, our data show that saccade-related cells are unaware of the blink-induced curvature of the eye movement and of the subsequent compensatory phase (Fig. 2; Goossens and Van Opstal 2000b). A similar dissociation between SC activity and the actual movement vector has been reported for saccades to remembered targets (Stanford and Sparks 1994) and for saccades elicited in a short-term adaptation paradigm (Frens and Van Opstal 1998). We thus propose that in our experiments compensation of the trajectory perturbation results from an error-corrective mechanism that acts downstream from the SC (see Fig. 3). Evidence for this was obtained in our previous study. If a pure blink-related eye movement is subtracted from the curved trajectory, a slow but straight eye movement results (Goossens and Van Opstal 2000a). In addition, SC cells did not respond to the blink-related eye movements (Goossens and Van Opstal 2000b).

Effects of SC lesions

According to our dynamic vector summation hypothesis, the instantaneous SC firing rates influence the velocity of the eye along its intended trajectory. The notion that each SC spike adds a tiny site-specific displacement vector to the movement command implies that eye velocity is not only influenced by the cell firing rates and their anatomical connection strengths with the brain stem, but also by the number of recruited cells. Indeed, it has been shown that when a subset of the active cell population is reversibly inactivated, saccade velocity is consistently reduced (Aizawa and Wurtz 1998; Lee et al. 1988; Quaia et al. 1998) and that these velocity deficits persist in the case of irreversible lesions (Hanes et al. 2005).

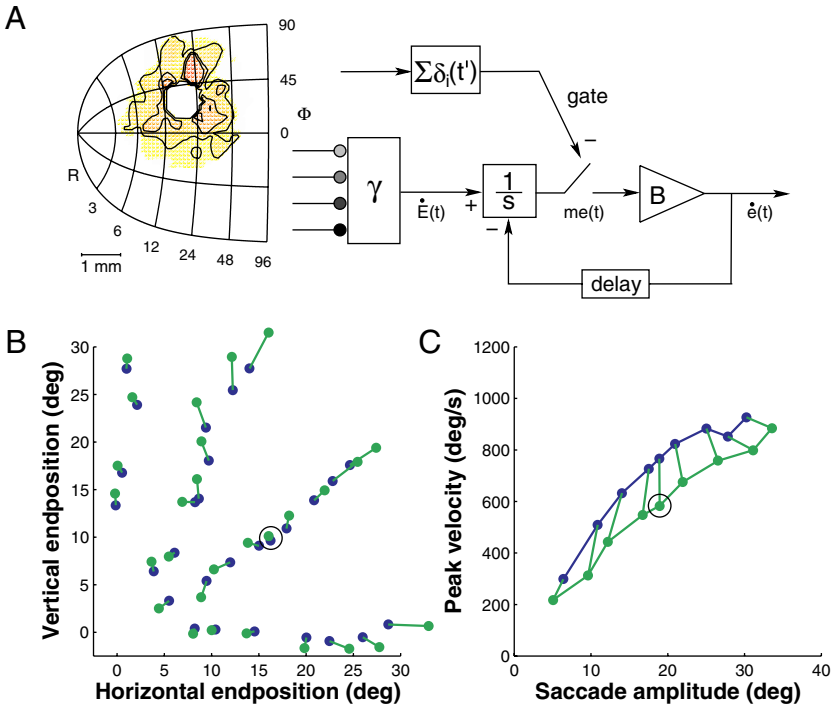

FIG. 10. Simulated SC lesions. *A*: extension of SC-brain stem model of Fig. 6 with an amplitude nonlinearity that ends saccade once total SC spike count, $\Sigma\delta_i(t')$, exceeds a fixed threshold. A 1-mm-diam hole in measured discharge patterns simulates a SC lesion at $[R,\Phi] = [19,30]°$. *B*: saccade endpoints with (green) and without (blue) lesion. ○, location corresponding to lesion site. *C*: peak velocity of control and lesion saccades in $\Phi = 30°$ direction. $\dot{E}(t)$, intended eye velocity; $me(t)$, dynamic motor error; $\dot{e}(t)$, current eye velocity. Values of model parameters were identical to ones in Fig. 6.

The changes in saccade metrics associated with reversible SC lesions have been interpreted to support the hypothesis that the saccade vector is specified by a weighted average of cell contributions rather than by linear vector summation (Lee et al. 1988). Interestingly, however, the dynamic vector-summation model can fully account for the observed SC lesion effects with one additional assumption, namely that the saccade is stopped once the total number of spikes from the SC population exceeds a fixed threshold. Indeed, many SC cells exhibit a considerable amount of postsaccadic activity that may last tens of milliseconds or more. Therefore the fixed number of spikes that contribute to control and perturbed saccades is often only a fraction of the total number of spikes produced by the cell (Goossens and Van Opstal 2000b; Matsuo et al. 2004). Furthermore, SC microstimulation experiments show that the amplitude of stimulation-evoked saccades increases with the number of stimulation impulses and with current strength, until it saturates at a site-specific value (Stanford et al. 1996; Van Opstal et al. 1990).

We thus extended the SC-brain stem model of Fig. 6 by letting this amplitude nonlinearity act downstream from the SC, and we simulated the effects of SC lesions by cutting a 1-mm-wide hole in the measured SC discharge patterns (Fig. 10*A*). This means that, after the lesion, the simulated movements ended when the total spike count from the remainder of the active population reached the same, fixed threshold for all saccades. This additional assumption is supported by our results shown in Fig. 7, *B* and *C*, which indicate that the unweighted sum of the population activity is roughly translation-invariant across the motor map. Note that the resulting changes in the metrics of the reconstructed saccades (Fig. 10*B*) were very similar to the ones observed after small lidocaine injections in the SC (Lee et al. 1988). That is, saccades to locations corresponding to the injection site were normometric, whereas the endpoints of saccades encoded by adjacent sites show a systematic deviation away from this location. Saccades encoded by sites rostral to the lesion were hypometric and those encoded by sites caudal to the lesion were hypermetric. Also, the concomitant decrease in eye velocity was readily reproduced in the simulations (Fig. 10*C*). Larger lesions (data not shown) produced hypometric saccades, such as observed after muscimol injections (Quaia et al. 1998), because the total number of SC spikes failed to reach the threshold. We conjecture that this threshold is under adaptive control, which would account for the altered movement fields after short-term adaptation of saccades (Frens and Van Opstal 1998) and the rapid recovery of amplitude deficits after small electrolytic lesions of the SC (Hanes et al. 2005).

The hypothesis thus entails that the localized SC population activity specifies a straight saccade trajectory until the brain stem saccade generator is stopped once the total number of spikes reaches a site-specific value. The latter control mechanism could be implemented by a parallel pathway through the cerebellum, which has been implicated in the control of saccade accuracy and movement duration by sending appropriately timed signals to the brain stem (Dean 1995; Fuchs et al. 1993; Ohtsuka and Noda 1995; Quaia et al. 1999; Thier et al. 2000, 2002).

Previous modeling studies have suggested that the effects of SC lesions on saccade metrics can also be reconciled with linear vector summation when intracollicular interactions are incorporated (Badler and Keller 2002; Bozis and Moschovakis 1998; Van Opstal and Van Gisbergen 1989). How SC inputs and intracollicular interactions may shape the SC movement fields, and thereby the SC population activity, is beyond the scope of this study.

Main sequence

Our finding that the nonlinear main sequence characteristics of the saccade kinematics may be fully determined by the spatial-temporal SC firing patterns is quite remarkable. Thus far, it has been widely assumed that the nonlinear main sequence properties of saccades are caused by saturation of burst-neuron firing rates in the brain stem. Interestingly, however, recent findings have suggested that an optimization principle could underlie these relations (Harris and Wolpert 1998). In line with this notion, our data suggest that the motor SC acts as a nonlinear vectorial pulse generator (Van Gisbergen and Van Opstal 1989; Van Gisbergen et al. 1985), which specifies the intended velocity of the eye along its optimal trajectory. The brain stem saccade generators can decompose this dynamic vectorial signal into appropriate commands for the eye muscles without the need of complex, vector-specific cross coupling between the horizontal and vertical pathways to produce straight movement trajectories in all directions (Smit et al. 1990). Note, however, that straight saccades are not built into the scheme of Fig. 6. In contrast to the "common source model" of Van Gisbergen et al. (1985), our new theory implies a multiple-source model in which each individual SC cell provides an independent dynamic contribution to the brain stem burst generators (*Eq. 8*). Each cell contributes a small straight eye displacement in the direction of its preferred vector, the amplitude of which depends on the number of spikes that the cell fires (as indicated by our analysis in Figs. 2, 4, and 5), but the trajectory encoded by the entire SC could be quite different from a straight eye movement. For example, under more complex visuomotor conditions (such as double-step target displacements or visual search tasks), the spatial-temporal distribution of SC activity could be such that the movement resulting from instantaneous linear vector addition is strongly curved (McPeek et al. 2003; Port and Wurtz 2003).

Burst and build-up cells

Hybrid feedback models of the SC have assigned specific—and qualitatively different—functional roles to saccade-related burst and build-up cells in the SC (Grossberg et al. 1997; Munoz and Wurtz 1995b; Wurtz and Optican 1994; Fig. 1*B*). However, accumulating evidence indicates that the response properties of these two subpopulations are not compatible with their presumed roles in the dynamic control of saccades (Anderson et al. 1998; Goossens and Van Opstal 2000b; Keller and Edelman 1994; Munoz et al. 1996; Port et al. 2000; Soetedjo et al. 2002a,b). Several experiments also have shown that the build-up activity of SC neurons can vary, in the same cell, from a significant level to essentially zero, depending on experimental conditions (Basso and Wurtz 1997; Dorris et al. 1997). Taken together, those data suggest that burst and build-up neurons are extremes of a continuum of neurons whose burst activity contributes similarly to the execution of a saccade. In line with this notion, we found a similar number of

spikes in the burst for control versus perturbed saccades in both cell types (Goossens and Van Opstal 2000b). Furthermore, our present analysis of the movement field dynamics yielded good quantitative descriptions of the burst discharge for both types of cells, resulting in a unimodal distribution of correlation values in Fig. 8*E*. Consistent with these results, and in line with previous observations (Anderson et al. 1998), we found that for each saccade, a single population of SC cells becomes active and that the activation site remains stationary on the SC motor map during saccade execution (Fig. 6).

In conclusion, our results show that the straight trajectories and nonlinear kinematics of saccades are already embedded in the dynamic ensemble activity of saccade-related SC cells and that the spatial-temporal SC firing patterns can be decoded by linear vector summation of the site-specific movement tendencies provided by each spike from the recruited population. As predicted by this dynamic ensemble-coding scheme, we found that the cumulative number of spikes in the burst of individual SC neurons is tightly related to the instantaneous displacement of the eye along its intended straight trajectory, both for normal saccades and for strongly perturbed saccades, and that this dynamic relation depends systematically on the saccade vector under both experimental conditions. Furthermore, we showed that the discharge dynamics of SC neurons can be predicted remarkably well from their classical, static movement fields using a novel dynamic movement field description. Our results thus yield a good quantitative description of the neural population code for saccades from the level of single spike events in individual SC neurons up to the animal's behavior.

ACKNOWLEDGMENTS

We thank H. Kleijnen and T. Van Dreumel for valuable technical assistance and F. Philipsen and A. Hanssen for preparing our monkeys.

GRANTS

This research was supported by the Dutch Foundation for the Life Sciences (project 805–01.072 to H.H.L.M. Goossens), the University of Nijmegen, the Netherlands to H.H.L.M. Goossens and A. J. Van Opstal, and the Human Frontiers Science Program (RG0174/1998-B to A. J. Van Opstal).

REFERENCES

Aizawa H and Wurtz RH. Reversible inactivation of monkey superior colliculus. I. Curvature of saccadic trajectory. *J Neurophysiol* 79: 2082–2096, 1998.

Anderson RW, Keller EL, Gandhi NJ, and Das S. Two-dimensional saccade-related population activity in superior colliculus in monkey. *J Neurophysiol* 80: 798–817, 1998.

Arai K and Keller EL. A model of the saccade-generating system that accounts for trajectory variations produced by competing visual stimuli. *Biol Cybern* 92: 21–37, 2005.

Badler JB and Keller EL. Decoding of a motor command vector from distributed activity in superior colliculus. *Biol Cybern* 86: 179–189, 2002.

Barton EJ, Nelson JS, Gandhi NJ, and Sparks DL. Effects of partial lidocaine inactivation of the paramedian pontine reticular formation on saccades of macaques. *J Neurophysiol* 90: 372–386, 2003.

Basso MA and Wurtz RH. Modulation of neuronal activity by target uncertainty. *Nature* 389: 66–69, 1997.

Berthoz A, Grantyn A, and Droulez J. Some collicular efferent neurons code saccadic eye velocity. *Neurosci Lett* 72: 289–294, 1986.

Bozis A and Moschovakis AK. Neural network simulations of the primate oculomotor system. III. A one-dimensional, one-directional model of the superior colliculus. *Biol Cybern* 79: 215–230, 1998.

Chimoto S, Iwamoto Y, Shimazu H, and Yoshida K. Monosynaptic activation of medium-lead burst neurons from the superior colliculus in the alert cat. *J Neurophysiol* 75: 2658–2661, 1996.

Cohen B and Henn V. Unit activity in the pontine reticular formation associated with eye movements. *Brain Res* 46: 403–410, 1972.

Dean P. Modelling the role of the cerebellum fastigial nuclei in producing accurate saccades: the importance of burst timing. *Neuroscience* 68: 1059–1077, 1995.

Dorris MC, Paré M, and Munoz DP. Neuronal activity in monkey superior colliculus related to the initiation of saccadic eye movements. *J Neurosci* 17: 8566–8579, 1997.

Edelman JA and Keller EL. Dependence on target configuration of express saccade-related activity in the primate superior colliculus. *J Neurophysiol* 80: 1407–1426, 1998.

Frens MA and Van Opstal AJ. Visual-auditory interactions modulate saccade-related activity in monkey superior colliculus. *Brain Res Bull* 46: 211–224, 1998.

Fuchs AF, Robinson FR, and Straube A. Role of the caudal fastigial nucleus in saccade generation. I. Neuronal discharge patterns. *J Neurophysiol* 70: 1723–1739, 1993.

Goossens HHLM and Van Opstal AJ. Blink-perturbed saccades in monkey. I. Behavioral analysis. *J Neurophysiol* 83: 3411–3429, 2000a.

Goossens HHLM and Van Opstal AJ. Blink-perturbed saccades in monkey. II. Superior colliculus activity. *J Neurophysiol* 83: 3430–3452, 2000b.

Groh JM. Converting neural signals from place codes to rate codes. *Biol Cybern* 85: 159–165, 2001.

Grossberg S, Roberts K, Aguilar M, and Bullock D. A neural model of multimodal adaptive saccadic eye movement control by superior colliculus. *J Neurosci* 17: 9706–9725, 1997.

Grossman GE and Robinson DA. Abmivalence in modeling oblique saccades. *Biol Cybern* 58: 13–18, 1988.

Guitton D, Bergeron A, Choi WY, and Matsuo S. On the feedback control of orienting gaze shifts made with eye and head movements. *Prog Brain Res* 142: 55–68, 2003.

Hanes DP, Smith MK, Optican LM, and Wurtz RH. Recovery of saccadic dysmetria following localized lesions in monkey superior colliculus. *Exp Brain Res* 160: 312–325, 2005.

Harris CM and Wolpert DM. Signal-dependent noise determines motor planning. *Nature* 394: 725–726, 1998.

Jürgens R, Becker W, and Kornhuber HH. Natural and drug-induced variations of velocity and duration of human saccadic eye movements: evidence for a control of the neural pulse generator by local feedback. *Biol Cybern* 39: 87–96, 1981.

Keller EL and Edelman JA. Use of interrupted saccade paradigm to study spatial and temporal dynamics of saccadic burst cells in the superior colliculus in monkey. *J Neurophysiol* 72: 2754–2770, 1994.

Keller EL, Gandhi NJ, and Vijay Sekaran S. Activity in deep intermediate layer collicular neurons during interrupted saccades. *Exp Brain Res* 130: 227–237, 2000.

Krauzlis RJ, Liston D, and Carello CD. Target selection and the superior colliculus: goals, choices and hypotheses. *Vision Res* 44: 1445–1451, 2004.

Lee C, Rohrer WH, and Sparks DL. Population coding of saccadic eye movement by neurons in the superior colliculus. *Nature* 332: 357–360, 1988.

Lefévre P and Galiana HL. Dynamic feedback to the superior colliculus in a neural network model of the gaze control system. *Neural Netw* 5: 871–890, 1992.

Matsuo S, Bergeron A, and Guitton D. Evidence for gaze feedback to the cat superior colliculus: discharges reflect gaze trajectory perturbations. *J Neurosci* 24: 2760–2773, 2004.

McPeek RM, Han JH, and Keller EL. Competition between saccade goals in the superior colliculus produces saccade curvature *J Neurophysiol* 89: 2577–2590, 2003.

Moschovakis AK, Kitama T, Dalezios Y, Petit J, Brandi AM, and Grantyn AA. An anatomical substrate for the spatiotemporal transformation. *J Neurosci* 18: 10219–10229, 1998.

Munoz DP, Pélisson D, and Guitton D. Movement of neural activity on the superior colliculus motor map during gaze shifts. *Science* 251: 1358–1360, 1991.

Munoz DP, Waitzman DM, and Wurtz RH. Activity of neurons in monkey superior colliculus during interrupted saccades. *J Neurophysiol* 75: 2562–2580, 1996.

Munoz DP and Wurtz RH. Saccade-related activity in monkey superior colliculus. I. Characteristics of burst and buildup cells. *J Neurophysiol* 73: 2313–2333, 1995a.

Munoz DP and Wurtz RH. Saccade-related activity in monkey superior colliculus. II. Spread of activity during saccades. *J Neurophysiol* 73: 2334–2348, 1995b.

Ohtsuka K and Noda H. Discharge properties of purkinje cells in the oculomotor vermis during visually guided saccades in the macaque monkey. *J Neurophysiol* 74: 1828–1840, 1995.

Ottes FP, Van Gisbergen JAM, and Eggermont JJ. Visuomotor fields of the superior colliculus: a quantitative model. *Vision Res* 12: 1795–1808, 1986.

Port NL, Sommer MA, and Wurtz RH. Multielectrode evidence for spreading of activity across the superior colliculus movement map. *J Neurophysiol* 84: 344–357, 2000.

Port NL and Wurtz RH. Sequential activity of simultaneously recorded neurons in the superior colliculus during curved saccades. *J Neurophysiol* 90: 1887–1903, 2003.

Quaia C, Aizawa H, Optican LM, and Wurtz RH. Reversible inactivation of monkey superior colliculus. II. Maps of saccadic deficits. *J Neurophysiol* 79: 2097–2110, 1998.

Quaia C, Lef´evre P, and Optican LM. Model of the control of saccades by superior colliculus and cerebellum. *J Neurophysiol* 82: 999–1018, 1999.

Scudder CA. A new local feedback model of the saccadic burst generator. *J Neurophysiol* 59: 1455–1475, 1988.

Scudder CA, Kaneko CRS, and Fuchs AF. The brainstem burst generator for saccadic eye movements: a modern synthesis. *Exp Brain Res* 142: 439–462, 2002.

Scudder CA, Moschovakis AK, Karabelas AB, and Highstein SM. Anatomy and physiology of saccadic long-lead burst neurons recorded in the alert squirrel monkey. I. Descending projections from the mesencephalon. *J Neurophysiol* 76: 332–352, 1996.

Smit AC, Van Opstal AJ, and Van Gisbergen JAM. Component stretching in fast and slow oblique saccades in the human. *Exp Brain Res* 81: 325–334, 1990.

Soetedjo R, Kaneko CRS, and Fuchs AF. Evidence against a moving hill in the superior colliculus during saccadic eye movements in the monkey *J Neurophysiol* 87: 2778–2789, 2002a.

Soetedjo R, Kaneko CRS, and Fuchs AF. Evidence that the superior colliculus participates in the feedback control of saccadic eye movements. *J Neurophysiol* 87: 679–695, 2002b.

Sparks DL. The brainstem control of saccadic eye movements. *Nat Rev* 3: 952–964, 2002.

Sparks DL and Hartwich-Young R. The deep layers of the superior colliculus. The neurobiology of saccadic eye movements. In: *Reviews of Oculomotor Research*, edited by Wurtz RH and Goldberg ME. Amsterdam: Elsevier, 1989, vol. 3, p. 213–255.

Sparks DL and Mays LE. Movement fields of saccade-related burst neurons in the monkey superior colliculus. *Exp Brain Res* 190: 39–50, 1980.

Stanford TR, Freedman EG, and Sparks DL. Site and parameters of microstimulation: evidence for independent effects on the properties of saccades evoked from the primate superior colliculus. *J Neurophysiol* 76: 3360–3381, 1996.

Stanford TR and Sparks DL. Systematic errors for saccades to remembered targets: evidence for a dissociation between saccade metrics and activity in the superior colliculus. *Vision Res* 34: 93–106, 1994.

Thier P, Dicke PW, Haas R, and Barash S. Encoding of movement time by populations of cerebellar Purkinje cells. *Nature* 405: 72–76, 2000.

Thier P, Dicke PW, Haas R, Thielert CD, and Catz N. The role of the oculomotor vermis in the control of saccadic eye movements. *Ann NY Acad Sci* 978: 50–62, 2002.

Van Gisbergen JA, Robinson DA, and Gielen S. A quantitative analysis of generation of saccadic eye movements by burst neurons. *J Neurophysiol* 45: 417–442, 1981.

Van Gisbergen JAM and Van Opstal AJ. Models. The neurobiology of saccadic eye movements. In: *Reviews of Oculomotor Research*, edited by Wurtz RH and Goldberg ME. Amsterdam: Elsevier, 1989, vol. 3, p. 69–98.

Van Gisbergen JAM, Van Opstal AJ, and Schoenmakers JJ. Experimental test of two models for the generation of oblique saccades. *Exp Brain Res* 57: 321–336, 1985.

Van Gisbergen JAM, Van Opstal AJ, and Tax AAM. Collicular ensemble coding of saccades based on vector summation. *Neuroscience* 21: 541–555, 1987.

Van Opstal AJ and Hepp K. A novel interpretation for the collicular role in saccade generation. *Biol Cybern* 73: 431–445, 1995.

Van Opstal AJ and Van Gisbergen JAM. A nonlinear model for collicular spatial interactions underlying the metrical properties of electrically elicited saccades. *Biol Cybern* 60: 171–183, 1989.

Van Opstal AJ and Van Gisbergen JAM. Role of monkey superior colliculus in saccade averaging. *Exp Brain Res* 79: 143–149, 1990.

Van Opstal AJ, Van Gisbergen JAM, and Smit AC. Comparison of saccades evoked by visual and collicular electrical stimulation in the alert monkey. *Exp Brain Res* 79: 299–312, 1990.

Waitzman DM, Ma TP, Optican LM, and Wurtz RH. Superior colliculus neurons mediate the dynamic characteristics of saccades. *J Neurophysiol* 66: 1716–1737, 1991.

Walton MM, Sparks DL, and Gandhi NJ. Simulations of saccade curvature by models that place superior colliculus upstream from the local feedback loop. *J Neurophysiol* 93: 2354–2358, 2005.

Wurtz RH and Optican LM. Superior colliculus cell types and models of saccade generation. *Curr Opin Neurobiol* 4: 857–861, 1994.